ELSEVIER

Applied Mathematical Modelling 22 (1998) 1059–1070

APPLIED MATHEMATICAL MODELLING

Computation of turbulent reactive flows in industrial burners

J. Ha *, Z. Zhu

CSIRO, Division of Mathematical & Information Sciences, Gate 7, 71 Normanby Road, Clayton-North 3169 Vic., Australia

Received 1 July 1997; received in revised form 17 March 1998; accepted 17 March 1998

Abstract

This paper presents models that are suitable for computing steady and unsteady gaseous combustion with finite rate chemistry. Reynold averaging and large eddy simulation (LES) techniques are used to model turbulence for the steady and unsteady cases, respectively. In LES, the Reynold stress terms are modelled by a linear combination of the scale-similarity and eddy dissipation models while the cross terms are of the scale-similarity type. In Reynold averaging, the conventional k–ϵ two-equation model is used. For the chemical reactions, a 3-step mechanism is used for methane oxidation and the extended Zeldovich and N_2O mechanism are used for NO formation. The combustion model is a hybrid model of the Arrhenius type and a modified eddy dissipation model to take into account the effects of reaction rate, flame stretch and turbulent intensity and scale. Numerical simulations of a flat pulse burner and a swirling burner are discussed.

Keywords: Turbulence; Chemistry; Pulse; Swirling; Burner

1. Introduction

In this paper, we will describe and present the results of some of our efforts in modelling turbulent combustion in the past few years. In particular, we will present models and simulation results of a flat pulse burner and a swirling burner. The chemical and physical processes that occur in such combustion systems are described by a system of conservation equations for mass, species, momentum and energy. They are time-dependent for the pulse burner but steady for the swirling burner. Solving these equations requires input data such as the species present, the chemical reactions that can occur, transport coefficients for viscosity, thermal diffusion, the equation of state for the various materials present and a set of boundary, source and initial conditions. In the next section, the governing equations for turbulent reactive flows, the combustion model and the kinetic mechanisms for methane and NO are presented. Using the model, results of numerical simulations of a flat pulse combustor and swirl burner are presented in Section 3.

2. Equations

The fluid dynamical and chemical properties of the system involving gas phase reactive flows obey the time-dependent conservation equations of mass, species, momentum and energy [1]. It is

* Corresponding author. Tel.: +61 3 9545 8000; fax: +61 3 9545 8080.

0307-904X/98/$ – see front matter
PII: S0307-904X(98)10042-2

generally accepted that these equations describe correctly the behaviour of the flow under both laminar and turbulent conditions. In principle, a "brute force" numerical solution of these equations would give the correct prediction of the flow behaviour, provided a sufficient spatial and time resolution is attained. The rapid increase of this required resolution with the Reynolds number rendered this impossible for problems of engineering interest. Consequently, the solutions to such problems must invariably be based on some form of turbulence modelling.

The great majority of current turbulence modelling work involves time (so-called Reynolds) averaging. In this only the mean field is resolved, with the entire eddy behaviour unresolved, and hence mathematically modelled. This approach is adopted for modelling turbulent swirling combustion. Time-averaging approaches tend not to work too well with transitional flows. An alternative to direct numerical simulation and time-averaging approaches is the large eddy simulation (LES). LES is used to model pulsating combustion.

In this section, models suitable for gaseous combustion of hydrocarbon fuel that are based on time-averaging and LES are presented as well as the combustion model and the kinetic mechanisms for methane and NO that we have adopted in our numerical simulations.

2.1. Large eddy simulation

In LES, it is assumed that the flow can be decomposed into two parts. The first part contains the large scale eddies. The second part contains the unresolved small scale eddies whose effects on the large scale eddies are modelled by subgrid scale (SGS) models. The governing equations of the large scale motion is obtained by spatial filtering. For compressible flows, the following two filtering procedures are used.

$$
\begin{aligned}
&\phi = \overline{\phi} + \phi', \\
&\overline{\phi} = \int_{\Omega} G(\mathbf{x}-\mathbf{z}, \Delta)\phi(\mathbf{z}, t)\, \mathrm{d}^3\mathbf{z}, \\
&\phi = \tilde{\phi} + \phi'', \\
&\overline{\rho\phi} = \overline{\rho}\tilde{\phi} = \int_{\Omega} G(\mathbf{x}-\mathbf{z}, \Delta)\rho(\mathbf{z}, t)\phi(\mathbf{z}, t)\, \mathrm{d}^3\mathbf{z},
\end{aligned}
$$

where ρ denotes, density, $\overline{\phi}$ and $\tilde{\phi}$ represent the filtered variables while ϕ' and ϕ'' are the SGS fields. The kernel $G(\mathbf{x}-\mathbf{z}, \Delta)$ is the filter function with a characteristic width Δ, and the integration is over the entire computational domain Ω. The second filtering procedure is known as Favre filtering. It was applied to LES by Erlbacher et al. [2] by extending the averaging technique introduced by Favre in traditional studies to compressible turbulence. Thus, the governing equations for the large scale components obtained by filtering are given by the following equations.

$$
\begin{aligned}
&\frac{\partial(\overline{\rho}\widetilde{Y_{\mathrm{A}}})}{\partial t} + \nabla\cdot(\overline{\rho}\widetilde{Y_{\mathrm{A}}}\tilde{\mathbf{v}}) = \overline{\omega_{\mathrm{A}}} - \nabla\cdot\left(\overline{\rho Y_{\mathrm{A}}\mathbf{V}_{\mathrm{A}}} + \mathbf{l}_{Y_{\mathrm{A}}} + \mathbf{c}_{Y_{\mathrm{A}}} + \mathbf{r}_{Y_{\mathrm{A}}}\right), \\
&\frac{\partial\overline{\rho}}{\partial t} = -\nabla\cdot(\overline{\rho}\tilde{\mathbf{v}}), \\
&\frac{\partial(\overline{\rho}\tilde{\mathbf{v}})}{\partial t} + \nabla\cdot(\overline{\rho}\tilde{\mathbf{v}}\tilde{\mathbf{v}}) = -\nabla\overline{P} + \nabla\cdot\left(\overline{\mathbf{S}} - \mathbf{L} - \mathbf{C} - \mathbf{R}\right), \\
&\frac{\partial(\overline{\rho}\tilde{h})}{\partial t} + \nabla\cdot(\overline{\rho}\tilde{h}\tilde{\mathbf{v}}) = \overline{\dot{P}} + \overline{\mathbf{S}\cdot\mathbf{D}} - \nabla\cdot(\overline{\mathbf{q}} + \mathbf{l}_h + \mathbf{c}_h + \mathbf{r}_h).
\end{aligned}
\tag{1}
$$

Here, t is time, $\mathbf{v}$ the velocity, Y_A the mass fraction of species A, ω_A the production rate, h the enthalpy, P the pressure, V_A the diffusion velocity, $\mathbf{S}$ the viscous stress tensor, $\mathbf{D}$ the rate of strain tensor and $\mathbf{q}$ the heat conduction vector. $\{\mathbf{L},\ \mathbf{l}_h,\ \mathbf{l}_{Y_A}\}$, $\{\mathbf{C},\ \mathbf{c}_h,\ \mathbf{c}_{Y_A}\}$ and $\{\mathbf{R},\ \mathbf{r}_h,\ \mathbf{r}_{Y_A}\}$ are the SGS Leonard, cross and Reynolds quantities.

The Leonard quantities can be calculated explicitly while both the cross and the Reynolds quantities have to be modelled. Although the Smagorinsky model is by far the most popular subgrid model, it is, however, absolutely dissipative, i.e. it cannot predict backscatter. Piomelli et al. [3] show that the transfer of energy between small and large scales is given by the SGS dissipation. Although energy is transferred from the large to the small scales (forwardscatter), reversed energy flow (backscatter) from the small scales to the large ones, associated with random fluctuations of the SGS stresses, does occur intermittently. The scale-similarity and mixed models of Bardina et al. [4] as well as the dynamic subgrid model of Germano et al. [5] are capable of predicting backscatter and thus are suitable for the transitional and non-equilibrium flows that we have here. Furthermore, Galilean invariance of the subgrid terms can be obtained for the scale-similarity model. The scale-similarity model does not ensure a net energy transfer from larger to smaller scales; thus it is used in linear combination with an eddy-viscosity model having the appropriate energy transfer properties. Thus

$$
\begin{aligned}
\mathbf{l}_{Y_A} &= \overline{\rho}(\widetilde{\widetilde{Y_A}\tilde{\mathbf{v}}} - \widetilde{Y_A}\tilde{\mathbf{v}}),\\
\mathbf{c}_{Y_A} &= c_{B3}\overline{\rho}(\widetilde{Y_A}\tilde{\mathbf{v}} - \widetilde{\widetilde{Y_A}}\tilde{\mathbf{v}}),\\
\mathbf{r}_{Y_A} &= -2c_Y\overline{\rho}\Delta^2||\tilde{\mathbf{D}}||\nabla\tilde{Y},\\
\mathbf{L} &= \overline{\rho}(\widetilde{\tilde{\mathbf{v}}\tilde{\mathbf{v}}} - \tilde{\mathbf{v}}\tilde{\mathbf{v}}),\\
\mathbf{C} &= c_{B1}\overline{\rho}(\widetilde{\tilde{\mathbf{v}}\tilde{\mathbf{v}}} - \widetilde{\tilde{\mathbf{v}}}\widetilde{\tilde{\mathbf{v}}}),\\
\mathbf{R} &= \overline{\rho}\Delta^2\left(\frac{2}{3}c_I||\tilde{\mathbf{D}}||^2\mathbf{I} - 2c_D||\tilde{\mathbf{D}}||\tilde{\mathbf{D}}_D\right),\\
\mathbf{l}_h &= \overline{\rho}(\widetilde{\tilde{h}\tilde{\mathbf{v}}} - \tilde{h}\tilde{\mathbf{v}}),\\
\mathbf{c}_h &= c_{B2}\overline{\rho}(\tilde{h}\tilde{\mathbf{v}} - \widetilde{\tilde{h}}\tilde{\mathbf{v}}),\\
\mathbf{r}_h &= -2c_H\overline{\rho}\Delta^2||\tilde{\mathbf{D}}||\nabla\tilde{h},
\end{aligned}
$$

where $||\cdot||$ is the Frobenius norm. Following Erlbacher et al. [2], the values of the dimensionless constants are assumed to have the following values: $c_I = 0.0066$, $c_D = 0.012$, $c_H = c_D/\mathrm{Pr_T} = 0.0133$ and $c_A = c_D/\mathrm{Sc_T} = 0.015$ where $\mathrm{Pr_T} \approx 0.9$ is the turbulent Prandtl number and $\mathrm{Sc_T} = 0.8$ is the turbulent Schmidt number. Bardina et al. [4] arrived at a value of $c_{B1} = 1.1$ by correlating with data obtained from direct numerical simulation of homogeneous isochoric non-reacting turbulent flow. However, in order to ensure that the transformation properties of $\mathbf{C}$ and $\mathbf{c}$ are the same when changing frame of reference c_{B1}, c_{B2} and c_{B3} must all equal unity.

Assuming that SGS fluctuations in the thermal conductivity and in the viscosities can be neglected in the flow results in the following approximate expressions for the diffusion vectors, the viscous stress tensor and the heat conduction vector.

$$
\begin{aligned}
\overline{\rho Y_A \mathbf{V}_A} &\approx -(\overline{D_A}\nabla\widetilde{Y_A} - \overline{\Theta_A}\nabla(\ln\ \tilde{T}))\widetilde{\mathbf{V}_A},\\
\overline{\mathbf{q}} &= \overline{\kappa\nabla T} = \overline{\kappa}\nabla\tilde{T} = (\overline{\kappa}/\overline{C_P})\nabla\tilde{h},
\end{aligned}
$$

where $\overline{D_A} = D_A(\overline{\rho}\tilde{T})$ is the mixture diffusion coefficients, $\overline{\Theta_A} = \Theta_A(\overline{\rho}, \tilde{T})$ the thermal diffusion ratios, and $\overline{\kappa} = \kappa(\overline{\rho}, \tilde{T})$ the thermal conductivity. The dissipation function and the substantive

time derivative of pressure of Eq. (1) can be calculated using the above equations. In this work, we choose to neglect the higher order correlations in the above equations and to calculate the dissipation function and the substantial time derivative of pressure according to: $\overline{\mathbf{S}\cdot\mathbf{D}} = \overline{\mathbf{S}}\cdot\tilde{\mathbf{D}}$ and $\dot{\overline{P}} = \partial_t(\overline{\rho}) + \tilde{\mathbf{v}}\cdot\nabla\overline{P}$.

2.2. k–ϵ turbulence models

The time-averaging of turbulent quantities in a combustion system leads to turbulence models for these quantities. In this paper, a conventional k–ϵ two-equation model will be used. This turbulence model relies on obtaining the value of turbulent kinetic energy k and a turbulent dissipation rate ϵ. Once k and ϵ are known, the turbulence viscosity μ_t can be calculated through a formula.

In the conventional k–ϵ turbulence model implemented in this paper, we first solve the transport equation for k

$$\rho\frac{\partial k}{\partial t} + (\rho\mathbf{V})\cdot\nabla k - \nabla\cdot[(\mu_0 + \tilde{\mu}_t/\sigma_k)\nabla k] = +\mu_t\sum_{i,j}\frac{\partial U_i}{\partial x_j}\left(\frac{\partial U_i}{\partial x_j} + \frac{\partial U_j}{\partial x_i}\right) - \rho\epsilon. \tag{2}$$

The dissipation rate ϵ is obtained by solving the equation

$$\begin{aligned}&\rho\frac{\partial\epsilon}{\partial t} + (\rho\mathbf{V})\cdot\nabla\epsilon - \nabla\cdot[(\mu_0 + \tilde{\mu}_t/\sigma_\epsilon)\nabla\epsilon]\\ &\quad = C_1\tilde{\mu}_t\frac{\epsilon}{k}\sum_{i,j}\frac{\partial U_i}{\partial x_j}\left(\frac{\partial U_i}{\partial x_j} + \frac{\partial U_j}{\partial x_i}\right) - \frac{2}{3}C_1\rho\epsilon(\bigtriangledown\cdot\mathbf{V}) - C_2\rho\frac{\epsilon^2}{k}.\end{aligned} \tag{3}$$

Here U_i is the ith component of the time-averaged velocity $\mathbf{V}$. $C_1 = 1.44$, $C_2 = 1.92$, $\sigma_k = 1.0$ and $\sigma_\epsilon = 1.3$, and $C_\mu = 0.09$.

The turbulence viscosity $\tilde{\mu}_t$ is calculated as

$$\tilde{\mu}_t = \rho\frac{C_\mu k^2}{\epsilon}. \tag{4}$$

The total viscosity with turbulence effects is computed as

$$\mu_t = \mu_0 + \tilde{\mu}_t,$$

where μ_0 is the fluid molecular viscosity.

For this conventional k–ϵ model, a wall-function treatment is needed for velocities along solid walls. In this paper, a log-law profile is imposed for the velocity components tangential to solid walls.

2.3. Combustion model

Chemistry makes itself felt in reactive flows through the mass supply terms ω_A that appear in the balance equations (1). Consider a system involving N constituents and M reaction steps,

$$\sum_{A=1}^{N} v_{Aj}^{R}\chi_A \rightarrow \sum_{A=1}^{N} v_{Aj}^{P}\chi_A, \quad j\in[1,\ldots,M],$$

where χ_A denotes the constituents and v_{Aj}^{R} and v_{Aj}^{P} are the stoichiometric coefficients for reactants and products of reaction j, respectively. For constituent χ_A, the contributions of all reactions may be expressed compactly as follows.

$$\omega_{\mathrm{A}} = M_{\mathrm{A}} \sum_{j=1}^{M} \left(v_{Aj}^{\mathrm{P}} - v_{Aj}^{\mathrm{R}} \right) \omega_j,$$

where ω_j denotes the reaction rate of reaction j and M_{A} is the molar mass of constituent A. A number of different modelling concepts are available for determining the rate of reaction, e.g. the eddy dissipation concept of Magnussen and Hjertager [6], the coherent flamelet models of Candel and Poinsot [7] and the thin flame model of Kerstin et al. [8]. In this work, the mass supply terms are taken to involve two simultaneous processes – chemical kinetics and SGS mixing. The rate determining process must then be the locally slowest process. Thus,

$$\omega_j = \min \left[\omega_j^{\mathrm{kin}},\ \omega_j^{\mathrm{mix}} \right].$$

Here, ω_j^{kin} denotes the kinetics controlled reaction rate according to the Arrhenius model.

$$\omega_j^{\mathrm{kin}} = k_j \prod_{A=1}^{N} Y_{\mathrm{A}}^{\sigma_{Aj}^{\mathrm{R}}},$$

where $k_j = A_j T^{\alpha_j} \exp(-E_j/(RT))$ is the modified Arrhenius rate constant for reaction j. Here, A_j is the pre-exponential factor, α_j the temperature exponent and E_j the activation energy. The σ_{Aj} are either the stoichiometric coefficients v_{Aj} if reaction j is a fundamental reaction or empirically determined numbers.

To estimate the SGS mixing controlled reaction rate ω_j^{mix}, the eddy dissipation model of Magnussen and Hjertager [6] is used.

$$\omega_j^{\mathrm{mix}} = \frac{\rho}{\tau_{\mathrm{mix}}} \min \left[Y_R / (v_{Rj}^{\mathrm{R}} M_R) \right],$$

where the superscript R denotes the reactants. Magnussen and Hjertager [6] proposed that chemical reactions take place when reactants are mixed on the molecular scale and have sufficiently high temperature and suggested that the characteristic time for SGS mixing $\tau_{\mathrm{mix}} \propto k/\epsilon$ where k is the turbulent kinetic energy and ϵ is its dissipation rate. Assuming $k \propto u'^2$ and $\epsilon \propto u'^3/\lambda_I$ where λ_I is the integral scale of turbulence, $\tau_{\mathrm{mix}} \propto \lambda_I/u'$ which is usually interpreted as a measure of the rate of strain. Furthermore, the quenching of flame at high strain rate is also an important phenomenon in combustion (Law et al. [9]). Thus, we assume that $\tau_{\mathrm{mix}} \propto 1/||\mathbf{D}||$, where $||\mathbf{D}||$ is the large scale rate of strain.

2.4. Chemical kinetics

Current models of methane oxidation involve up to 20 species and over 100 elementary reactions [10]. Because of the large number of species and elementary reactions in the complete reaction mechanism for methane, it is difficult to implement in computational flow models. Numerical calculations involving complete methane reaction mechanism is also expensive to carry out. One strategy for reducing the computational effort is to use reduced mechanisms obtained on the basis of steady-state, equilibrium and partial equilibrium assumptions, reduction in the computing effort, mainly because of the of species involved.

The single-step mechanism predicts flame speed reliably over considerable ranges of conditions but it has several flaws. By assuming that the reaction products are CO_2 and H_2O, the total extent of reaction will be overpredicted. At adiabatic flame temperature typical of hydrocarbon fuels (about 2000 K) substantial amount of CO and H_2 exist in equilibrium with CO_2 and H_2O. This equilibrium lowers the heat of reaction and the adiabatic flame temperature T_{ad} below the values predicted by the single global reaction. Over-estimate of T_{ad} grows with increase in equivalence

ratio. In addition to effects of equilibrium composition in the product gases, single mechanism also neglects the fact that typical hydrocarbon fuels burn in a somewhat sequential manner. That is, fuel is partially oxidised to CO and H_2 which are not appreciably consumed until all of the hydrocarbon species have disappeared. Thus, we use the following three-step mechanism of Westbrook and Dryer [10] for methane combustion in our work.

$$CH_4 + \tfrac{1}{2}O_2 \rightarrow CO + 2H_2,$$
$$CO + \tfrac{1}{2}O_2 \leftrightarrow CO_2,$$
$$H_2 + \tfrac{1}{2}O_2 \rightarrow H_2O.$$

For engineering applications, there is also a strong need for reliable prediction of NO. In this paper, the following extended Zeldovich and N_2O mechanisms are used for the formation of NO and the method of Rokke et al. [11] is used for their computation.

$$O + N_2 \leftrightarrow NO + N,$$
$$N + O_2 \leftrightarrow NO + O,$$
$$N + OH \leftrightarrow NO + H,$$
$$N_2 + O + M \leftrightarrow N_2O + M,$$
$$N_2O + O \leftrightarrow 2NO,$$
$$N_2O + O \leftrightarrow N_2 + O_2,$$
$$N_2O + H \leftrightarrow N_2 + OH.$$

3. Numerical simulations

3.1. Pulsating combustion

Here, some of the results about the operational, flow and combustion characteristics of pulse combustors that can be extracted from numerical simulation based on the LES model of Section 2.1 will be presented. An outline of the burner of 0.04 m thickness used in the calculations is given in Fig. 1. A typical operation of a pulse combustor is the periodic intakes of fuel and air in response to the pressure oscillations in the combustion chamber. Many factors can affect the operating frequency of the burner. Factors that increase the pulsation frequency include lower heat transfer, higher injection velocity, shorter tailpipe length and higher heat release rate. For example, doubling the firing rate of the burner from 110 to 220 MJ/h raises the operating frequency of the flat burner from 57 to 66 Hz. The spectral contents of pressure also change. The

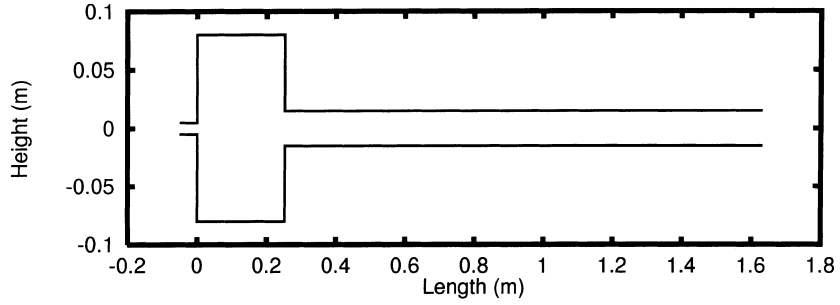

Fig. 1. Geometry of the pulse combustor.

amplitudes of the frequencies other than the dominant frequency and its harmonics are higher in the higher firing rate case than those in the lower firing rate case. This may be explained by the fact that combustion is more intense and the pressure waves radiated from the combustion "pockets" are stronger in the case of higher firing rate than in the case of lower firing rate. This gives rise to beating in the pressure time series. The beat phenomenon is caused by the interference between the bulk pressure oscillation and the pressure waves radiated from the combustion pockets. This observation has an important implication on the design of pulse combustors for engineering application. It is expected that tuning pulse burners of high firing rates require more effort than that for low firing rates.

The computed velocity field of Fig. 2 shows the presence of a number of vortices. The vortex structure was found to be responsible for the macroscopic convection and mixing of the reactants with the residual hot products. They are also important in determining the combustion characteristics [12]. It was found that combustion never completely stops but diminishes towards the end of the cycle and that it occurs in pockets. The temporal and spatial patterns of these pockets are strongly influenced by the vortex structure of the flow.

The periodic increase in pressure in the combustion chamber must follow closely the periodic increase in heat release for stable operation of a pulse combustor. Many factors can affect the phase relation between pressure and heat release. The oxidation of hydrocarbon to CO marks the beginning of the overall energy release. The formation of this intermediate thus determines the time delay to significant energy release. The flame quenching effect at high strain rate also plays a role in affecting the time delay.

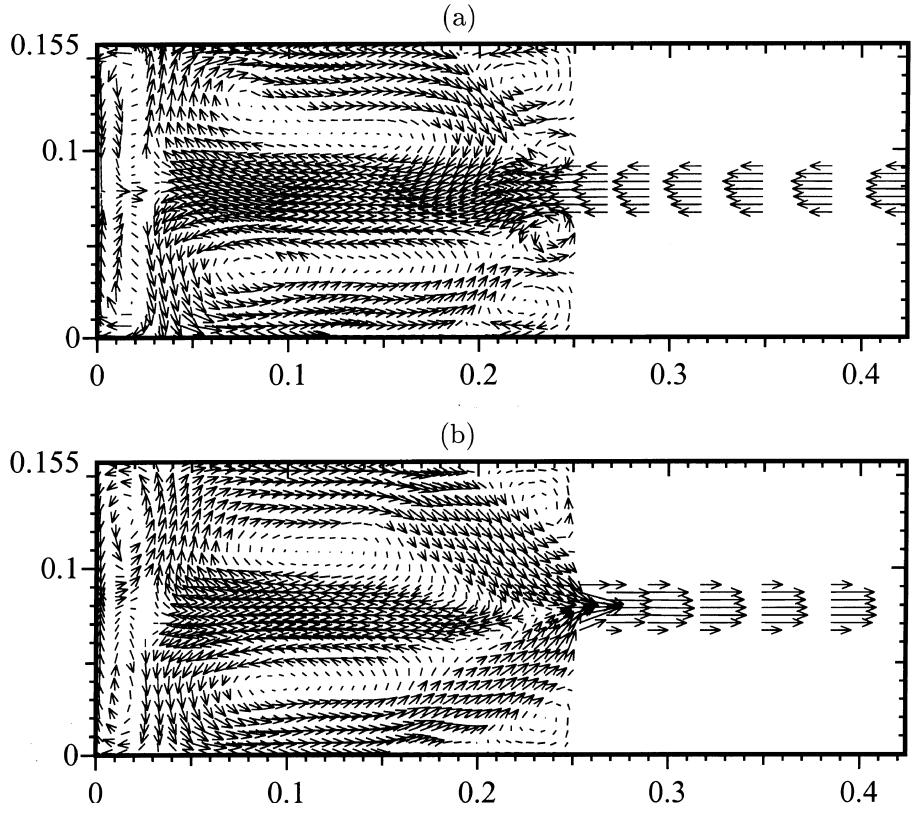

Fig. 2. Velocity at: (a) the end of injection and (b) the peak of reaction.

3.2. Swirling combustion

For complex swirling flows with combustion, numerical simulations in the time-averaging approach are within easy reach of most workstations in terms of computational time and memory requirement. A turbulent combusting flow inside a furnace [13] is predicted with the turbulence model of Section 2.2 and the combustion model of Section 2.3.

The axi-symmetric burner is a model furnace with swirling natural gas flame inside. The furnace and burner arrangement are illustrated in Fig. 3. The incoming air has a large swirl number of $S_w = 0.85$ at the annulus inlet (indicating the ratio between the tangential and axial velocity components at the inlet). We choose the radius $R = 0.15$ m of the burner as the characteristic length, the mean axial velocity $U = 13.7$ m/s at the air annulus inlet is taken as the characteristic velocity. The Reynolds number is thus $\mathrm{Re} = 139\,081$, the Mach number is $\mathrm{Ma} = 0.047$. Since the flow is axi-symmetric, the domain $0 < r, R, 0 < x < X$ is considered. The domain is covered by a total of 4165 four-node bilinear elements.

In Fig. 4, the right half cross-section gives the computed velocity arrows superimposed with streamlines, while the left half section illustrates temperature gray-scale plot. In this figure, we can clearly see that in the region close to the fuel inlet, there is a very large area of flow reversal. This is due to the sudden expansion caused by the combustion. This large zone of flow reversal is also

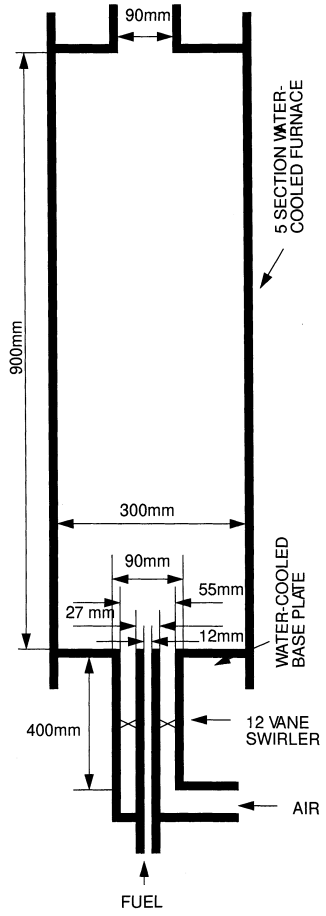

Fig. 3. Furnace enclosure and coaxial burner.

observed in experiment. For the gray-scale plot of temperature in the left half cross-section, dark scale indicates high temperature. This plot shows that a flame front is extended from the fuel inlet toward the outer furnace wall, and high temperature is more confined in a region close to the furnace outer wall and within the axial segment of $0.8 < X/R < 2.1$.

Fig. 5 gives the comparison between the computed temperature and experimental data along the central axis of the furnace. We can see that the predicted temperature is in very good agreement with experimental data in regard to the maximum temperature value and its location. Apart from the region close to the fuel inlet where the experimental results are under-predicted, the numerical solution gives a very accurate simulation. In Fig. 6, we compare computed axial velocity with experimental data at four axial (X) locations along the burner axis. At $X = 0.03$ m, the computed solution resembles experimental data closely but the flow reversal near the axis is not predicted accurately. Similar conclusion can be drawn for the $X = 0.05$ m location. At $X = 0.1$ m, the flow reversal close to the axis is well predicted. For $X = 0.3$ m, the computed solutions agree very well with experimental data.

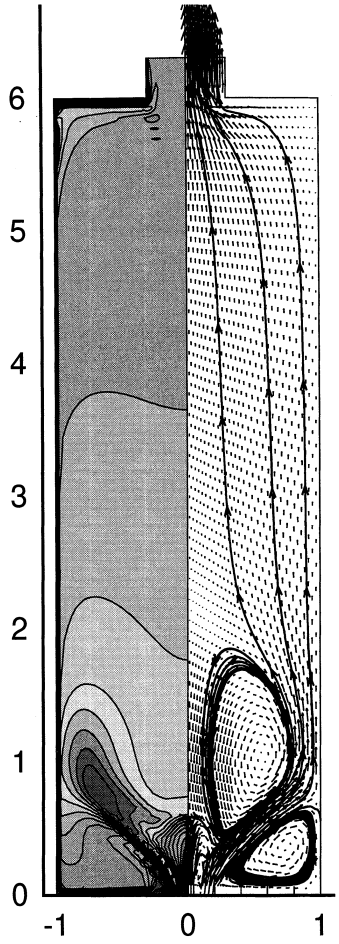

Fig. 4. Velocity arrows are shown in the right half cross-section, and the temperature gray-scale is shown in the left half cross-section.

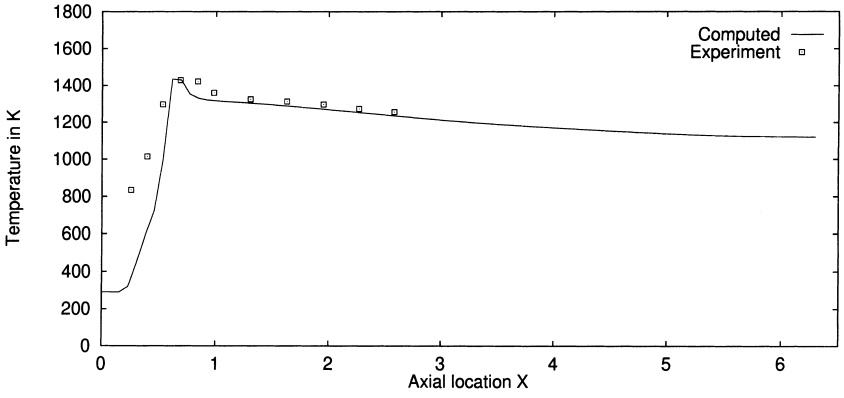

Fig. 5. Temperature comparison along the furnace axis.

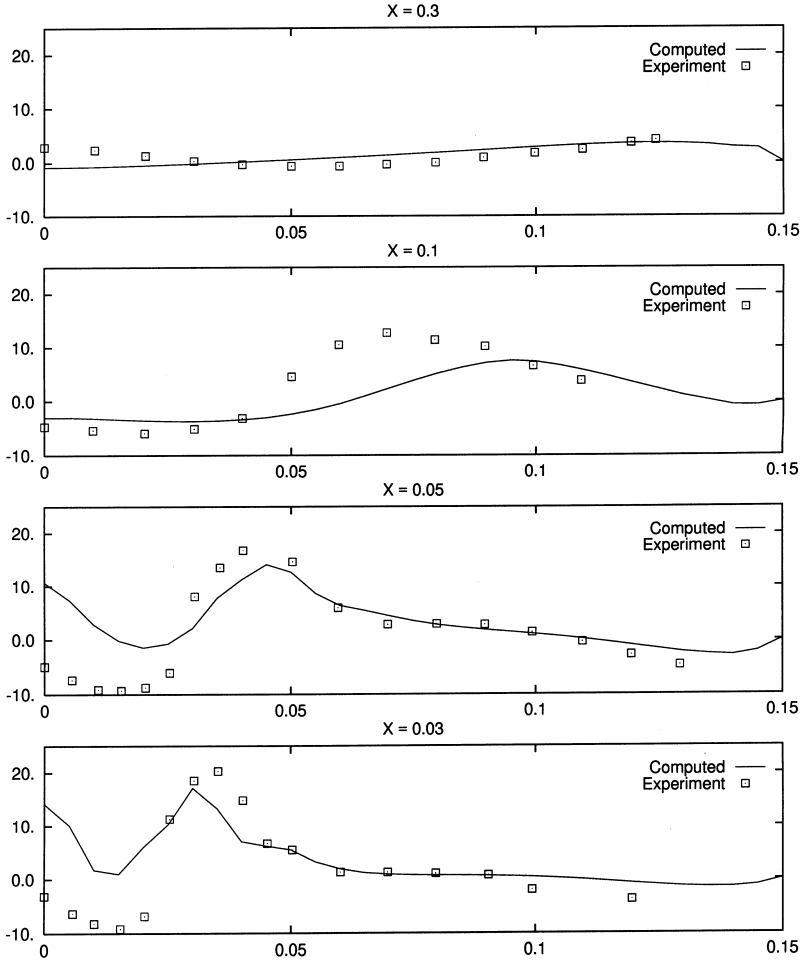

Fig. 6. Comparison of axial velocity component along the furnace axis.

4. Conclusion

The models presented in Section 2 are suitable for modelling compressible premixed and non-premixed reactive flows. LES was used by Ha [12] to study the flow and combustion characteristics of pulsating combustion where the fuel and air are premixed before injecting into the combustor. Here, the model was applied to a parametric study to extract information about the various influences that affect pulsating combustion. The vortex structure and its relation with the combustion characteristics demonstrate the strong coupling between fluid dynamics and chemical reactions.

With a k–ϵ turbulence model and a 3-step combustion model, we have obtained the solution for a complex swirling flow with combustion in a burner. As shown in Figs. 5 and 6, the accuracy of the simulation is satisfactory, a large improvement to the earlier work by Zhu and Stokes [14]. As the numerical algorithm for the Reynolds averaging approach is implemented in the Finite-Element package *Fastflo*, we can easily predict flows with combustion in complex geometries often encountered in the mineral and power generation industries.

Acknowledgements

J. Ha thanks C. Fureby of the Swedish National Defence Research Establishment and his colleagues at the CSIRO Division of Building, Construction and Engineering for many helpful discussions. The swirling combustion work was first sponsored by BHP Research, and completed as a combustion module of the general PDE package *Fastflo*.

References

[1] E.S. Oran, J.P. Boris, Numerical Simulation of Reactive Flow, Elsevier, New York, 1987.
[2] G. Erlbacher et al., Toward the large-eddy simulation of compressible turbulent flows, J. Fluid Mech. 238 (1992) 155–185.
[3] U. Piomelli, H. Cabot, P. Moin, S. Lee, Subgrid-scale backscatter in turbulent and transitional flows, Phys. Fluids A 3 (1991) 1766–1771.
[4] J. Bardina, J.H. Ferziger, W.C. Reynolds, Improved turbulence models based on large eddy simulation of homogeneous incompressible turbulent flows, Report No. TF-19, Stanford University, Stanford, CA, 1983.
[5] M. Germano et al., A dynamic subgrid-scale eddy viscosity model, Phys. Fluids 29 (1986) 1755.
[6] B.F. Magnussen, B.H. Hjertager, On mathematical modelling of turbulent combustion with special emphasis on soot formation and combustion, in: 18th International Symposium on Combustion, Combustion Institute, 1976, pp. 719–727.
[7] S.M. Candel, T.J. Poinsot, Flame stretch and the balance equation for the flame area, Combust. Sci. Technol. 70 (1990) 1–15.
[8] A. Kerstin, W.T. Ashurst, F.A. William, Field equation for interface propagation in an unsteady homogeneous flow field, Phys. Rev. A 37 (1988) 2728.
[9] C.K. Law, D.L. Zhu, G. Yee, Propagation and extinction of stretched premixed flames, in: 21st International Symposium on Combustion, Combustion Institute, 1988, pp. 1419–1426.
[10] C.K. Westbrook, F.L. Dryer, Chemical kinetic modeling of hydrocarbon combustion, Prog. Energy Combust. Sci. 10 (1984) 1–57.
[11] N.A. Rokke et al., Scaling of nitric oxide emissions from buoyancy dominated hydrocarbon turbulent-jet diffusion flame, in: 24th International Symposium on Combustion, Combustion Institute, 1992, pp. 385–393.
[12] J. Ha, Numerical studies of a flat pulse combustor, in: Proceedings of Comput. Tech. and Appl. Conference, 1995, pp. 359–366.

[13] J. Sykes, J.S. Truelove, A finite difference computer program for calculating turbulent and combusting fluid flows, AERE Report No. R 9485, Harwell, 1979.
[14] Z. Zhu, N. Stokes, Computation of turbulent combustion flows with a finite-element method, Computational Techniques and Applications: CTAC95, 1995, pp. 855–862.